Chapter 2

MPFEM Modeling on the Compaction of Al/SiC Composite Powders with Core/Shell Structure

Xizhong An, Yu Liu, Fen Huang and Qian Jia

Additional information is available at the end of the chapter

http://dx.doi.org/10.5772/intechopen.76563

Abstract

Uniaxial die compaction of two-dimensional (2D) Al/SiC core/shell (core: SiC; shell: Al) composite powders with different initial packing structures was numerically reproduced using DEM-FEM coupled MPFEM modeling from particulate scale. The effects of external pressure, initial packing structure, and SiC content on the packing densification were systematically presented. Various macro and micro properties such as relative density and distribution, stress and distribution, particle rearrangement (e.g. sliding and rolling), deformation and mass transfer, and interfacial behavior within composite particles were characterized and analyzed. The results show that by properly controlling the initial packing structure, pressure, and SiC content, various anisotropic and isotropic Al/SiC particulate composites with high relative densities and uniform density/stress distributions can be obtained. At early stage of the compaction, the densification mechanism mainly lies in the particle rearrangement driven by the low interparticle forces. In addition to sliding, accompanied particle rolling also plays an important role. With the increase of the compaction pressure, the force network based on SiC cores leads to extrusion on Al shells between two cores, contributing to mass transfer and pore filling. During compaction, the debonding between the core and shell of each composite particle appears and then disappears gradually in the final compact.

Keywords: Al/SiC composite powders, compaction, core/shell structure, MPFEM modeling, debonding and rebonding

1. Introduction

Among the advanced particulate reinforced metal matrix composites (PRMMCs), Al/SiC composite is the most commonly studied one due to its potentially high tensile strength and

elastic modulus at room or elevated temperatures, low thermal expansion coefficient, high thermal and electrical conductivity, excellent corrosion resistance, good wear resistance, mechanical properties, ductility, low cost and wide range of applications [1–3]. Normally, two routes (i.e. powder metallurgy (PM) and melt based approach) are used to fabricate PRMMCs with 'net shape' or 'near-net shape' forming. In the fabrication of Al/SiC composites via a melt process, SiC often reacts with molten Al to degrade the reinforcement strength and the interfacial strength [4], and the uniform distribution of SiC particles especially those with nanosizes are difficult to be realized. This deficiency can be largely avoided by PM process which can offer more control over reinforcement distribution and require less energy input than the conventional foundry route. A common PM process of Al/SiC composite consists of cold compaction in a closed-die or in an isostatic pressing followed by sintering. To fabricate Al/SiC composites with superior performances, large amount of physical and numerical work was carried out using PM method in the past few decades.

Physically, many researchers studied the effects of SiC content and particulate sizes using various forming methods. Ling et al. carried out experiments to study the PM fabrication of Al/SiC composites with SiC content ranging from 0 to 30 vol.% (volume fraction), where four PM methods (such as sintered, cold isostatic pressed (CIPed) and sintered, hot isostatic pressed (HIPed), and sintered plus HIPed in the same HIP cycle) were considered and the results of relative density, mechanical properties, and fractography were characterized and compared [1]. They found that the sintered plus HIPed technique can yield the best bulk composites. When the SiC content is within 10 vol.%, the matrix is more likely suffered to ductile failure. With a higher SiC content, the factors such as the interfacial bond strength, pore structure evolution, and the cracking within particles can all determine the mechanical properties of the composite products. For the Al/SiC composite powder comprising 40 vol.% SiC, Sridhar and Fleck respectively performed isostatic and closed-die compaction [5]. They found that for a given SiC powder content, the compaction pressure to achieve a given relative density increases with the decrease of the SiC particle size. The measured yield surfaces after each compaction indicated that the shape depends on the deformation path, with greatest hardening along the loading direction. Tavakoli et al. [2] studied the consolidation behavior of Al/SiC composite powders (with reinforcement SiC up to 50 vol.%) during pressure cycling (ranging from 90 to 360 MPa with 1 Hz) at room temperature in uniaxial compaction experiments to address the effects of compaction mode and SiC content on the densification, microstructure and mechanical properties of Al/SiC composites. And corresponding comparisons were made with monotonic compaction. The results showed that the pressure cycling can enhance the densification of Al/SiC composite powder, and the densification rate increases with the SiC content. Using HIP, Tang et al. [6, 7] studied the consolidation of Al/SiC composite powder with 6.5 vol.% nano-sized SiC particles (25 nm in size) synthesized via cryomilling and followed by hot rolling. Microstructural investigation indicated that the nano-sized SiC particles had been dispersed homogeneously in the reinforced regions in the composites and the tensile strength of the composite was improved greatly. However, coarse-grained SiC_p-free regions were observed to be formed during HIPing, which improved the ductility but to a certain degree decreased the strength. In short, SiC nanoparticles located at grain boundaries can contribute to limiting grain growth, but it is difficult to achieve the complete uniform

distribution of nano SiC particles. Jamaati et al. [8] investigated the effects of SiC particle size (2 and 40 μm, respectively) on microstructure and mechanical properties (tensile strength and elongation) of Al/SiC (with 10 vol.% SiC) composite fabricated by accumulative roll bonding. It was found that the composite strip with 40 μm particle size became uniform with high bonding quality and without any porosity sooner than the strip of 2 μm particle size. For both sizes, different cycles could lead to different tensile strength and tensile elongation.

To determine the compressibility behavior of Al-Cu/SiC composite powder mixtures which include 4 wt.% (weight fraction) Cu and 5–20 wt.% SiC, a double action die compaction with the pressure ranging from 50 to 450 MPa was performed by Ghiţă and Popescu [9]. And empirical equations were proposed to describe densification mechanism of the composite powders and predict the optimal pressure applied. Li et al. [10] carried out physical experiments to study the distributions of SiC particles in different positions of the Al/SiC composite samples (with 35 vol.% SiC) formed by equal channel angular pressing and torsion (ECAPT) and found that the shear strain could create significant influences. And from the compaction stage to the angular pressing stage during ECAPT, the distribution homogeneity of SiC particles increases greatly, implying that this forming method can realize relatively homogeneous SiC distribution. With the addition of nanosized SiC particles (0–7 wt.%), Moazami-Goudariz and Akhlaghi [11] conducted physical experiments on the compaction of Al/SiC composites. In their work, the effects of morphology, microstructure, size, apparent density, flowability, and hardness of the produced powder mixtures on their compaction behavior were investigated. The results showed that the chemical composition and the nano SiC content created effects on the compaction behavior as well as properties of the compact. Al/SiC composites with different contents (up to 15 vol.%) and sizes (3, 6, and 11 μm) of SiC particles were fabricated using conventional PM route [12], where the effects of the size and content of SiC particulates on the microstructural and corrosion behavior of the composite were studied. Meanwhile, El-Kady and Fathy [13] also studied the effects of SiC particle size (70 nm, 10, and 40 μm) and content (5 and 10 wt.%) on both physical and mechanical properties of Al/SiC nanocomposites produced with PM followed by hot extrusion. Majzoobi et al. [14] investigated the tribological properties of Al/SiC nanocomposite prepared by hot dynamic compaction (with the strain rate of 10^3 s^{-1}), where the content of SiC nanoparticles was respectively 0, 5, and 10 vol.%. After compaction, the relative density of the composite compact can be up to 98%.

Recently, the mechanical properties and corrosion behavior of Al/SiC (comprising 20 vol.% SiC) composites fabricated by vacuum hot pressing sintering at 700°C under a pressure of 20 MPa were studied by Zhang et al. [15], in their work the high relative density of 99.65 ± 0.08% for the Al/SiC composite can be obtained. Cold isostatic compaction of Al/SiC composite powders with different content of nano SiC particulates as the reinforcement was experimentally performed by Bajpai et al. [16], where various properties such as hardness, density, porosity, compressive strength, indirect tensile strength and the microstructure of the samples were measured and characterized. The micrograph shows the uniform distribution of nano SiC particles in the aluminum matrix. With micro wave sintering and hot extrusion, Penchal Reddy et al. [17] fabricated nano-sized SiC (0, 0.3, 0.5, 1.0 and 1.5 vol.%) reinforced Al metal matrix composites and studied the structural, mechanical and thermal properties of the developed Al/SiC nanocomposites. Results indicated that hot extruded

Al/SiC nanocomposites (with 1.5 vol.% SiC) exhibited the best mechanical and thermal performance as compared to the other developed Al/SiC nanocomposites.

Aforementioned researches in physical experiments indicate that most of the previous work was mainly focusing on the sintering stage or the forming stage, comprehensive studies on the compaction of Al/SiC composite powders are less conducted. Actually, most of the densification takes place in the compaction stage by rate-independent plasticity [1]. And the relative density (defined as the volume of the powder divided by the volume occupied by the die) and corresponding packing structure of the compact can determine the subsequent sintering process as well as the final properties of the sintered component. Therefore, the researches on the compaction of Al/SiC composite powders when subjected to external energy have increasingly attracted the materials scientists and engineers' interests in the past few years. Nevertheless, even though physical experiments can reproduce the relationship between relative density and compaction pressure and/or temperature, they are unable to quantitatively characterize the local density distribution, stress distribution, and particle motion behavior for pore (or void) filling in situ, especially the nonlinearity features in geometry, materials, and contact during compaction all increase the difficulties of physical experiments [18–22]. Most importantly, it's really hard for researchers to accurately control the uniform distribution (ordered or disordered) of reinforcement (SiC) in the metal (Al) matrix, these disadvantages in physical experiments can be conquered by the so called numerical simulations.

Numerically, various models or methods were proposed or used to simulate powder compaction densification in PM process. For example, a traditional macro continuous FEM (finite element method) simulation model, in which the powder mass is regarded as a continuum with uniform void distribution, was proposed to solve the problems arising from physical experiments. In addition to the relationship between overall relative density and compaction pressure, this method can also be used to analyze local relative density and distribution, stress distribution, and powder displacement in the compact upon compaction from macro continuous scale. Therefore, as reported in the authors' previous researches, the single-action die compaction of pure metal powders [23, 24] and composite powders [25] has been systematically investigated by this method. Even though the traditional FEM can to some extent solve the problems in physical experiments, it is really hard to deal with the important issues like dynamics and contact mechanics from particulate scale based on the aforementioned continuum assumptions. However, this will be overcome by molecular dynamics based DEM (discrete element method) simulation. DEM has been widely applied to generate various packing structures of spherical and non-spherical particles [26–29], but its effectiveness in modeling the compaction of powders is restricted to limited relative density (e.g. $\rho < 0.85$) [30]. For higher relative density and extra large plastic deformation in PM compaction, a new method MPFEM (multi-particle FEM) has been developed and successfully applied in modeling this process [31–43], but less work was conducted on the compaction of Al/SiC composite powders from particulate scale. Recently, using MPFEM the authors successfully modeled the single action die compaction of Al/SiC composite mixtures [44], and the results show that the packing state, size and number of SiC particles in the initial packing structure can significantly influence not only the densification of the Al/SiC composite powders upon compaction but also the properties of the compacts. Even though our previous numerical simulation can reproduce the compaction of

Al/SiC binary powder mixtures, there are still some problems left unsolved, which include: (1) it's really difficult to precisely control the distribution of SiC reinforced particles; (2) it cannot realize full densification especially when SiC particles formed agglomeration or clusters; (3) the local density and stress distributions in the compact are non-uniform. With these problems, a new binary Al/SiC composite constructed by the compaction of powders with core (SiC)/shell (Al) structures were designed and the whole process was simulated by MPFEM method from particulate scale. Currently, no relative literature has been found.

In this chapter, uniaxial die compaction of Al/SiC composite core/shell powders with different initial packing structures was numerically reproduced using DEM-FEM coupled MPFEM modeling from particulate scale. The effects of external pressure, initial packing structure, and SiC content (composition) on the packing densification were systematically presented. Various macro and micro properties such as relative density and distribution, stress and distribution, particle rearrangement (e.g. sliding and rolling), deformation and mass transfer, and interface behavior between particles were characterized and analyzed. Some interesting results have been obtained, which can provide the materials scientists and engineers with valuable references to the realization of fully dense and high performance Al/SiC composite compacts in PM production.

2. Simulation method and conditions

2.1. Simulation method

The simulation method used in current work is MPFEM. In this method, the initial random powder packing is firstly generated by DEM and then imported into FEM model, where each particle is fully discretized into finite element meshes. **Figure 1** respectively gives the schematic diagram of an individual composite particle with core/shell structure and corresponding mesh division as well as the numerically generated initial packing structure in the closed die before compaction when the SiC content is 25 vol.%, where each core (SiC)/shell (Al) composite particle includes respectively 200/1700 nodes and 173/1552 elements. After all the parameters and conditions are determined, the program will be complied and run in the commercialized MSC.Marc software. For simplicity, the details of DEM model are not given here, interested readers can refer to [26–29, 45] for more information. In comparison, each initial ordered binary packing is generated by the intrinsic function in MSC.Marc software based on geometry. The initial random or ordered packing structure was then imported into MPFEM model as the input. **Figure 2** shows the packing morphologies of Al/SiC composite powders before compaction. Here three initial ordered packings, i.e. simple cubic (SC), hexagonal close packed (HCP) and honeycomb structures are considered. The composition of the composite powder can be adjusted by the thickness of Al shell, which is represented by $R - r$, where R and r are respectively the radius of the composite Al/SiC particle and the radius of SiC particle therein. It needs to clarify that the SiC content used in this chapter all refers to volume fraction. For each initial packing structure before compaction, corresponding parameters such as the size ratio between the radius of SiC particle and the radius of the whole composite particle (r/R), SiC content (vol.%), and packing density (or relative density) are listed in **Table 1**.

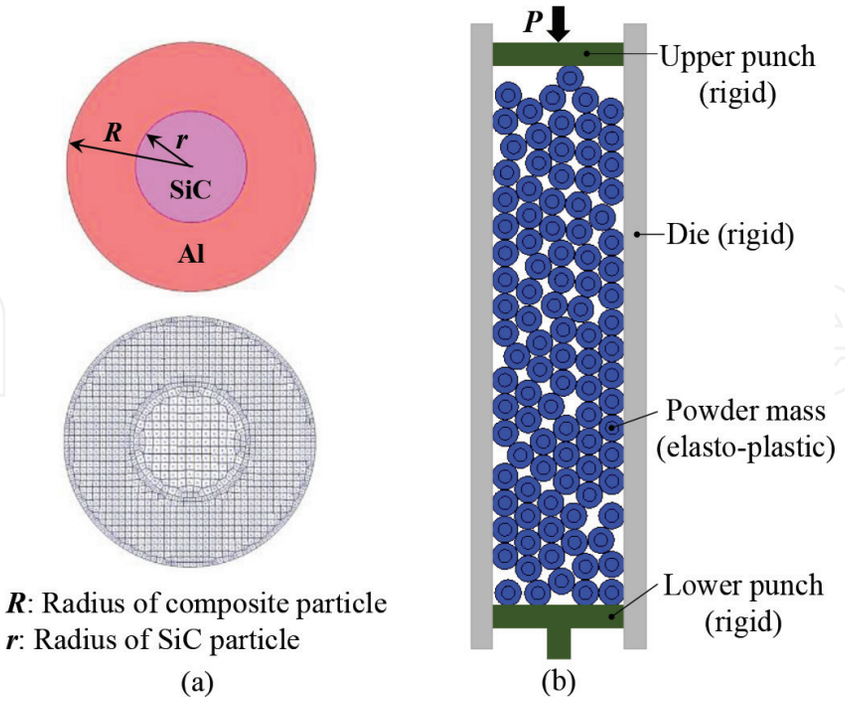

Figure 1. (a) Schematic diagram of an individual Al/SiC composite particle with core/shell structure and mesh division used in MPFEM simulation; (b) DEM generated initial packing structure in a closed die before compaction with 25% SiC.

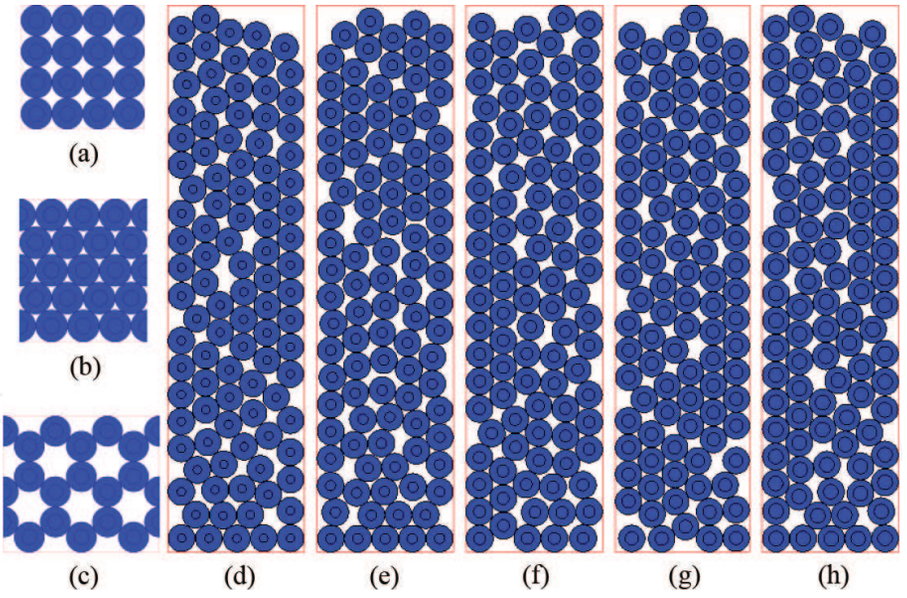

Figure 2. Initial packing structures of Al/SiC composite particles before compaction, where: (a) SC packing; (b) HCP packing; (c) honeycomb packing; (d)–(h) represent random packings with the SiC content of 10, 15, 20, 25, and 30% in volume fraction.

2.2. Simulation conditions

After the generated binary initial packing structure was imported into the MPFEM model in MSC. Marc software, the simulation conditions including material properties, definition of contact,

http://dx.doi.org/10.5772/intechopen.76563

Initial packing structure	Size ratio (*r*/*R*)	SiC content, vol.%	Packing density
SC	1/2	25	0.7841
SC	2/3	44.4	0.7842
HCP	1/2	25	0.8782
HCP	2/3	44.4	0.8783
Honeycomb	1/2	25	0.6045
Random	1/√10	10	0.7516
Random	√15/10	15	0.7526
Random	1/√5	20	0.7544
Random	1/2	25	0.7424
Random	√3/√10	30	0.7515

Table 1. Corresponding parameters for initial packing structures of composite powders before compaction.

mesh adaptability, and loading cases etc. were then set. In the simulation, the power law model is used to describe the properties of aluminum materials and the yield stress is given by:

$$\sigma_y = \mathrm{A}\left(\varepsilon_0 + \bar{\varepsilon}\right)^{\mathrm{m}} + \mathrm{B}\,\dot{\bar{\varepsilon}}^{\mathrm{n}} \tag{1}$$

where A, B, m, n are material constants; ε_0 is the initial yield strain; $\bar{\varepsilon}$ is the equivalent strain; $\dot{\bar{\varepsilon}}$ is equivalent strain rate. Initially, $\bar{\varepsilon}$ and $\dot{\bar{\varepsilon}}$ are assumed to be zero. Therefore, the initial yield strain can be expressed as:

$$\varepsilon_0 = (E/\mathrm{A})^{1/(\mathrm{m}-1)} \tag{2}$$

where E is Young's modulus. The equivalent strain rate is:

$$\dot{\bar{\varepsilon}} = \left[2/3\left(\varepsilon_{\mathrm{ij}}\,\varepsilon_{\mathrm{ij}}\right)\right]^{1/2} \tag{3}$$

where $\varepsilon_{\mathrm{ij}}$ is the strain tensor. The material parameters and modeling parameters are respectively given in **Tables 2** and **3**. Here, SiC material was assumed to be elastomer due to its high hardness compared with Al. In the simulation, the upper punch is movable, while the lower

Materials	Young's modulus, *E*/GPa	Poisson's ratio, ν	Strength coefficient, A/MPa	Work hardening index, m
Al	70.00	0.33	225.90	0.05
SiC	470.00	0.142	Elastic-perfectly	

Table 2. Materials parameters used in the simulation.

Contact definition	Loading setup	Operation conditions
Particles: deformable	Iteration method: full Newton-Raphson algorithm	Friction: modified Coulomb friction model
Die and punches: rigid	Convergence criteria: displacement or residual stress control	Large deformation: updated Lagrange function
Friction coefficient between particles: $\mu = 0.2$	Global mesh self-adaptive division: for Al part	Contact method: segment to segment method
Upper punch: velocity control ($v = 1$ mm/s)		

Table 3. Modeling parameters used in the simulation.

punch and the die are fixed. During compaction, the relative density of the compact is calculated by the displacement of the upper punch, and it is not influenced by the strain rate because the materials are set to be not sensitive to this parameter. Meanwhile, each Al granular mesh was set to global mesh self-adaptive to guarantee the accuracy of simulation results. Once all the simulation parameters are determined, the job will be submitted to the server for running.

3. Results and discussion

3.1. Compaction process and property characterization

In PM production, the relationship between the relative density ρ and the pressure P during compaction is always firstly concerned. Here, the compaction curves ($\rho - P$ relations) for different ordered packings of composite Al/SiC powders are shown in **Figure 3**, where the inset images demonstrate the morphologies of the compacts at different compaction stages (marked by A, B, and C) with honeycomb initial packing structure. As can be seen that before compaction, different ordered packing structures correspond to different initial relative densities. For SC and HCP initial packings, both the relative densities increase smoothly with the compaction pressure to a high value. While for the compaction on honeycomb initial packing, the fluctuation of relative density during pressing can be observed when the pressure is very low. This can be explained by: (1) For SC and HCP initial packings, their structures are stable. During compaction the densification is mainly achieved by plastic deformation of Al component, little relative sliding and rolling between Al/SiC composite particles can be observed. Therefore, the compaction curves evolve smoothly; (2) Compared with SC and HCP, honeycomb initial packing structure is less stable. So at the early stage of compaction, the initial ordered packing structure is destroyed (please refer to the evolution of packing morphology in the inset images of **Figure 3(a)** for details, where the arrows indicate the tendency of movement for corresponding particles and the circled areas illustrate the local dense clusters formed after rearrangement), which leads to the rearrangement of the composite particles through sliding and rolling for densification. And this process continues until all the particles are in a stable state. From **Figure 3(a)** one can also find that even the initial

http://dx.doi.org/10.5772/intechopen.76563

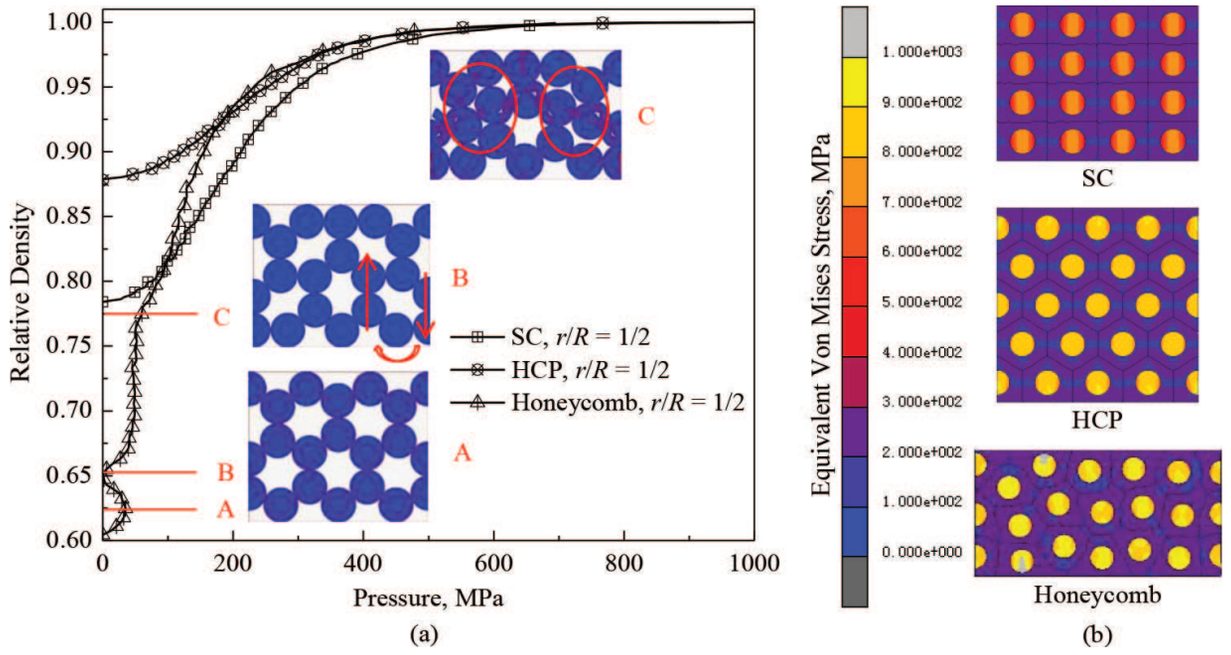

Figure 3. (a) Evolution of relative density with the pressure during compaction of different initial ordered packing structures, where the inset figures are the morphologies of compacts from honeycomb initial packing at different compaction stages; (b) morphologies of final compacts obtained in (a) and corresponding stress distributions.

packing structures are different, the compaction in each case can reach almost full densification with the relative density of about 1.0 for each compact, which exhibits the advantages of the Al/SiC composite powders with core/shell structures. However, the structures of final compacts and the distributions of stresses therein as indicated in **Figure 3(b)** all demonstrate different features. Especially for the compact obtained from honeycomb initial ordered packing, the shape of each composite particle and the distribution of equivalent Von Mises stresses are all non-uniform compared with the former two cases and more like disordered state, which will determine the final performance of the compact.

In comparison with ordered initial packings, the initial random packings of Al/SiC composite powders are frequently encountered in actual PM production. **Figure 4** gives the compaction curves of five initial random packings with different SiC contents and relative densities as well as corresponding model validation. As indicated in **Figure 4(a)**, the compaction curves are quite different from those in **Figure 3(a)**, which can be ascribed to the difference of initial packing structures. For each $\rho - P$ curve during compaction on random initial packing, three stages can be identified: (1) At the initial compaction stage with very low pressure, the densification is mainly implemented by particle rearrangement to fill the large voids or pores. Here, the translational motion and rotational motion of the particles are dominant in densification. (2) Once a stable packing is formed in the first stage, the compaction steps into the second stage for large deformation. At this stage, the relative density of the compact increases continuously with the pressure due to the plastic deformation of Al component for adjacent pore filling, which greatly increases the relative density. (3) When the pressure exceeds a critical value, the increasing rate of the relative density decreases, and each $\rho - P$ curve tends to level off because the large deformation of particles creates work hardening which impedes further

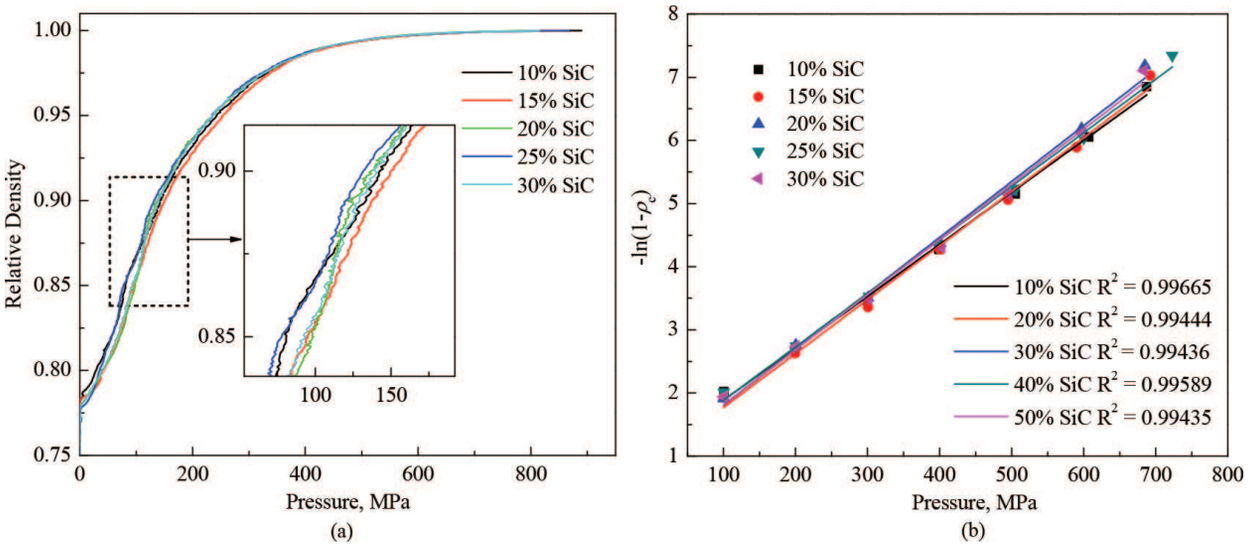

Figure 4. (a) Compaction curves for five initial random packings with different SiC contents, where the inset figure shows the local zoom of the compaction curves; (b) validation of the numerical model by fitting the simulation results with the Heckel equation (b).

deformation unless extra high pressure is applied. In this stage, the powder mass shows a bulk behavior. In order to validate the effectiveness of the model used in the simulation, the numerical results are fitted with Heckel equation given by [46, 47]:

$$\ln\left[1/(1-\rho_c)\right] = UP + Z \tag{4}$$

where ρ_c is the relative density of the compact; P is applied pressure; U and Z are constants. **Figure 4(b)** demonstrates that the simulation results agree well with the Heckel equation with high confidence (high R^2 value), which proves the robustness of the numerical model and the accuracy of the simulation results. It needs to note that both the differences of compaction curves as shown in the enlarged zoon of **Figure 4(a)** and of the slopes of the fitting lines as indicated in **Figure 4(b)** can be influenced by the initial packing structure and SiC content. But compared with the compaction on ordered initial packing structures, the influences of SiC content on the densification behavior are less significant, which will be discussed in the subsequent sections.

3.2. Initial packing structure effects

Previous results have illustrated that the initial packing structure of the composite powder or the SiC content can create effects on the compaction behavior and property of the compact. To further identify their important role in the densification process, the compaction on SC and HCP ordered initial packings with different SiC contents is shown in **Figure 5**, where **Figure 5(a)** gives the compaction curves and **Figure 5(b)** indicates the morphologies of the compacts under the pressure of 200 MPa and the stress distributions therein. Here, the equivalent Von Mises stress is given by:

$$\bar{\sigma} = \left[(\sigma_1-\sigma_2)^2+(\sigma_2-\sigma_3)^2+(\sigma_3-\sigma_1)^2\right]^{1/2}/\sqrt{2} \tag{5}$$

http://dx.doi.org/10.5772/intechopen.76563

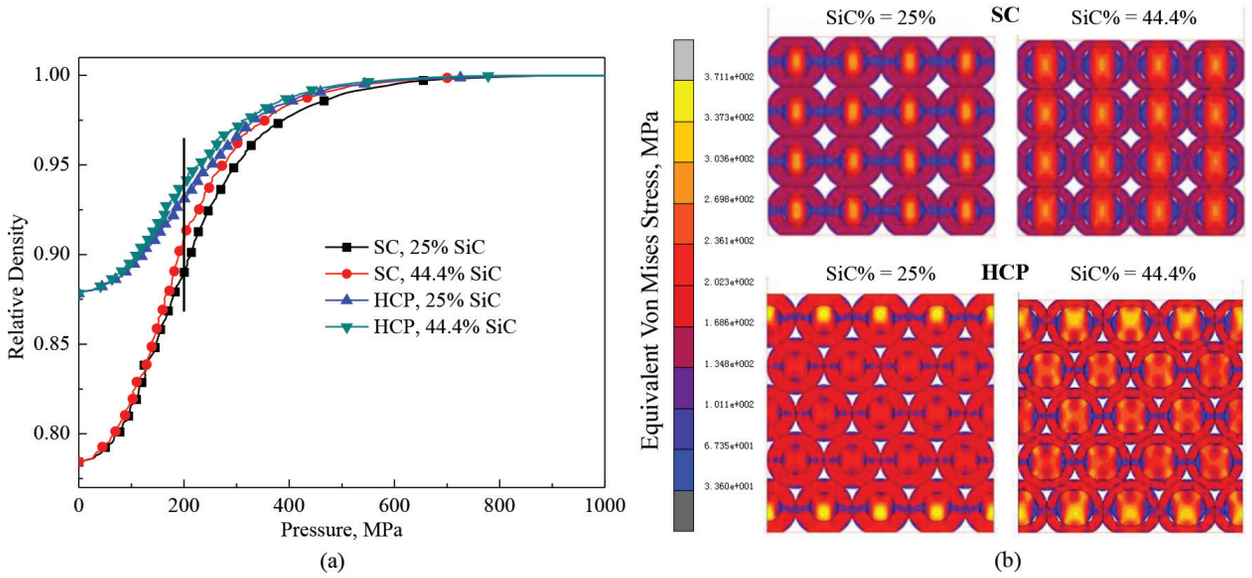

Figure 5. (a) Compaction on SC and HCP ordered initial packing structures with different SiC contents; (b) equivalent Von Mises stress distributions in the compacts formed from SC and HCP initial packings with respectively 25 and 44.4% SiC when the compaction pressure is 200 MPa.

where σ_1, σ_2, σ_3 are the principal Cauchy stresses along three main axes. It can be seen that the compaction on different initial packing structures can lead to different densification behavior and rate. For the same initial packing structure, increasing the SiC content can aid the densification. I.e. with a certain compaction pressure, the relative density of the compact with high SiC content is larger than that with low SiC content. This can be explained by the high efficient stress transmission as indicated in **Figure 5(b)** when P = 200 MPa. One can see that larger stresses are mainly concentrated on SiC particles (cores) in the compacts with higher SiC content, which can accelerate the densification through mass transfer by adjacent Al deformation extruded by neighboring SiC cores. Compared with the compacts obtained from SC initial packing, the stresses in corresponding compacts with HCP structure are larger, which implies the higher densification rate for the latter case. Meanwhile, from **Figure 5(b)** one can also find that debonding at the interface between Al and SiC occurs for both cases when the SiC content is high, the mechanism of this phenomenon can be discussed in the following section.

In addition to the compaction on ordered initial packing structures, the evolutions of morphologies and stresses in the compacts formed by random initial packings with five SiC contents at different compaction stages are also systematically studied. Here, the compaction on the random initial packing with 25% SiC is taken as an example for detailed analysis. **Figure 6** gives the morphology evolution of the compact and corresponding stress transmission/distribution at each compaction stage. As indicated, during compaction both translational motion (including the sliding as indicated by the arrow in the third snapshot of **Figure 6(a)**) and rotational motion are observed, which are mainly occurred in early stage of compaction when the pressure is low. In this case, the densification is mainly due to the rearrangement of the Al/SiC composite particles, and the force chain is formed as a skeleton or network. With the increase of the incremental modeling steps N, the particles that form the force network begin to deform when the pressure exceeds their yield limit. Due to the heterogeneity of the force

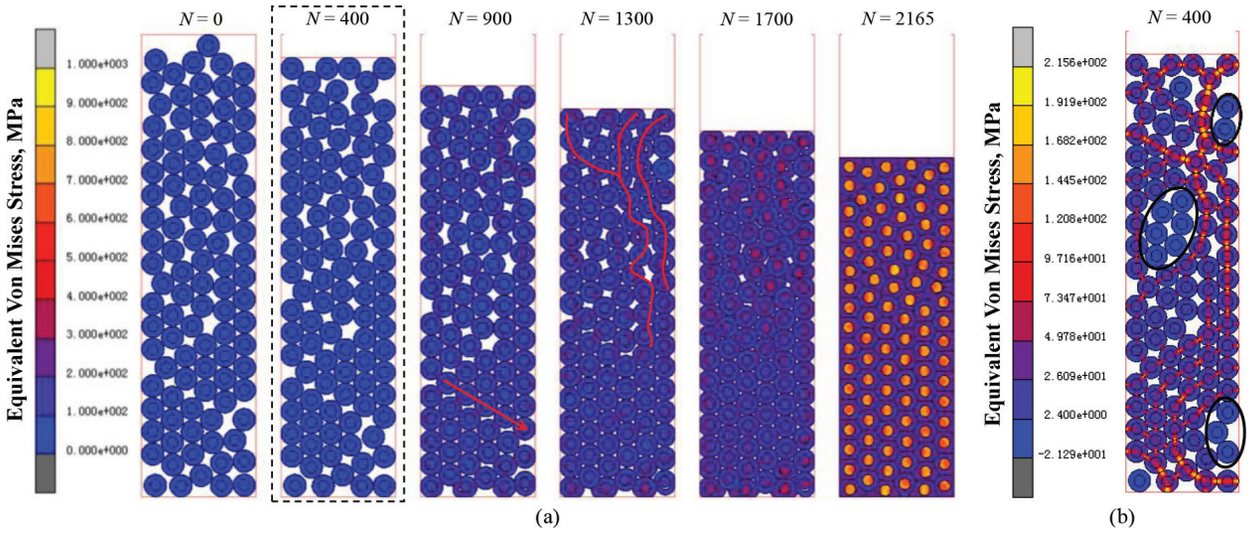

Figure 6. (a) Evolution of equivalent Von Mises stresses during compaction on random initial packing with 25% SiC; (b) force chain structure and stress transmission in the compact when the incremental modeling step is $N = 400$, where the circled local structures are the clusters surrounded by the force chains, within which no or only small stresses can be identified in these particles.

structure, the shape of each composite particle in the final compact is irregular. In the whole process, the force chain structure varies, which dominates the deformation of the particles and the stresses are mainly concentrated on SiC particles. To more clearly demonstrate the force chain structure and explain the irregular deformation of the composite Al/SiC particles, the compact obtained at the incremental modeling step $N = 400$ in **Figure 6(a)** is redisplayed while the scale of the legend is reduced as shown in **Figure 6(b)**. From the figure one can see that not all of the particles in the compact are involved in the force chain, some local clusters as circled are shielded by the force chain which makes them free from deformation, because the forces or stresses on these particles are very small or even nil, which will impede the densification process. On the other hand, the particles in the force chain are easily moved or deformed by the large forces acted on them, which will enhance the densification. On the whole, due to the non-uniformity of the force chain and stress distributions, even though the final compact can be fully dense, the deformation of the composite particles therein is not uniform. This phenomenon has been identified in the MPFEM modeling on the compaction of Fe-Al composite powders [42]. While unlike the compaction on mixed binary Al and SiC composite powders, the reinforced SiC particles are uniformly distributed in the fully dense final compact and the stress distributions are also homogeneous, which indicates the advantages of current process applied in PM production.

3.3. Quantitative analysis on particle rearrangement during compaction

It is known that the densification of composite powders during early stage of compaction is mainly due to the rearrangement of particles through translational motion and rotational motion, while systematic analysis on the particle rotation in the compaction process is less studied because this behavior is difficult to be quantitatively characterized. To achieve this, an algorithm is proposed to calculate the rotation of particles during compaction. **Figure 7(a)**

http://dx.doi.org/10.5772/intechopen.76563

schematically illustrates the particle (here two nodes adjacent to SiC core in Al is selected as the research target) relative position before (e.g. ΔOAB) and after (e.g. ΔOA′B′) rotation, here the coordinates of (x_A, y_A) for point A, (x_B, y_B) for point B, (x_A', y_A') for point A′, (x_B', y_B') for point B′ are known at each time step. Therefore, the rotational angle θ can be calculated by:

$$\theta = \alpha + \beta \tag{6}$$

where:

$$\alpha = \tan^{-1}\left(\frac{y_B - y_A}{x_B - x_A}\right) \tag{7}$$

and

$$\beta = \tan^{-1}\left(\frac{y_B' - y_A'}{x_B' - x_A'}\right) \tag{8}$$

To further study the effects of initial packing structures, three packings with the similar relative densities (≈ 0.74) and SiC (25%) but different structures as shown in **Figure 7(b)** were chosen for analysis. The results are shown in **Figure 8**, where **Figure 8(a)** gives the evolution of average rational angle with the relative density of each initial packing structure during compaction and **Figure 8(b)** indicates the quantitative statistics on the distribution of rotational angles. As can be seen from **Figure 8(a)** that with each case, the average rotational angle increases with the relative density but the increasing rate decreases. And different initial packing structures

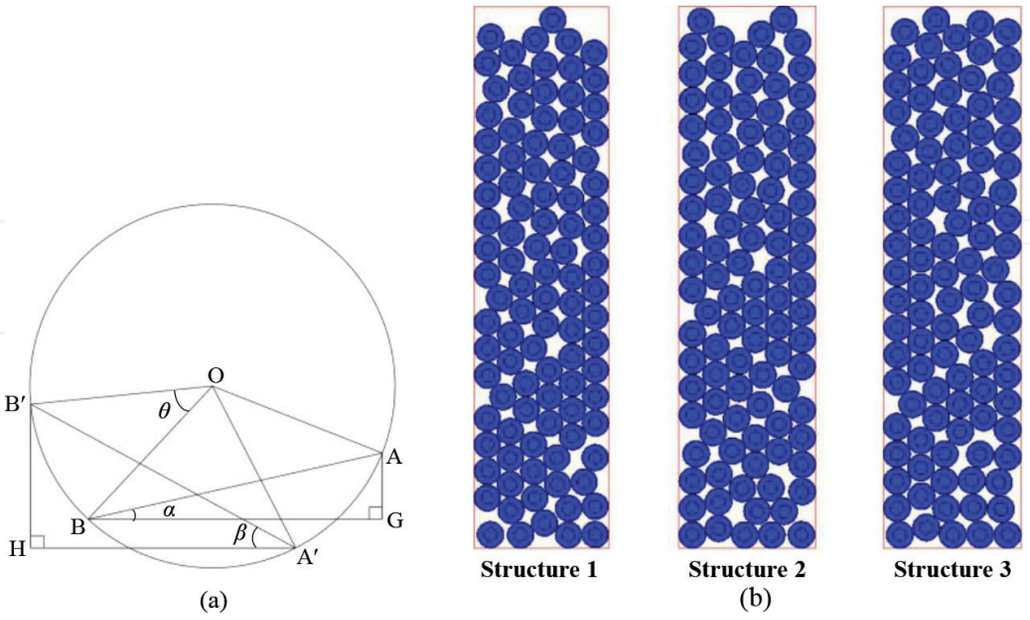

Figure 7. (a) Schematic diagram to calculate the rotation of one particle during compaction; (b) three initial packing structures with similar relative density and SiC content (25%) but different packing structures used for quantitative particle rotation calculation during compaction.

can result in different rotation behavior even the relative density and the composition of the composite powder are similar. Meanwhile, one can also find that the fast increasing region of rational angle is mainly located in the region where the relative density is lower than about 0.82. Previous researches [48] have demonstrated that 0.82 is the relative density of random close packing state with stable structure for 2D disks, beyond which both the translational motion and rotational motion during compaction become difficult. This variation has similar trend with previous results from other packing systems [31]. Besides, the distribution of average rotation angle in **Figure 8(b)** indicate that during compaction most particles rotate with the angle of 1–5°. Large scale particle rotation is mainly formed at the initial rearrangement stage of the compaction when the pressure is low. Because after deformation under high pressure the contact between neighboring particles changes from point to face, which restrains the further rotation of composite particles. From **Figure 8(b)** one can also find that different initial packing structures can lead to different rotation behavior, which will further determine the densification process as well as the resultant properties of the final compacts.

3.4. Debonding and rebonding phenomena

During compaction on composite powders with core/shell structures, a common phenomenon, i.e. debonding can be occurred, which has also been observed at the Al/SiC interface in current MPFEM simulation. Interestingly, after debonding, the separated Al and SiC in a composite particle can rebond again to form a good cohesion and combination at the interface. It needs to clarify that in current simulation only physical interaction at the interface is considered, chemical reactions are not included. Previous results in this chapter have shown that some composite particles are debonded during compaction. Especially for those particles that are close to the punches or close to the large voids, the debonding is more probable. Those composite particles that form local ordered dense packing structure are not likely to

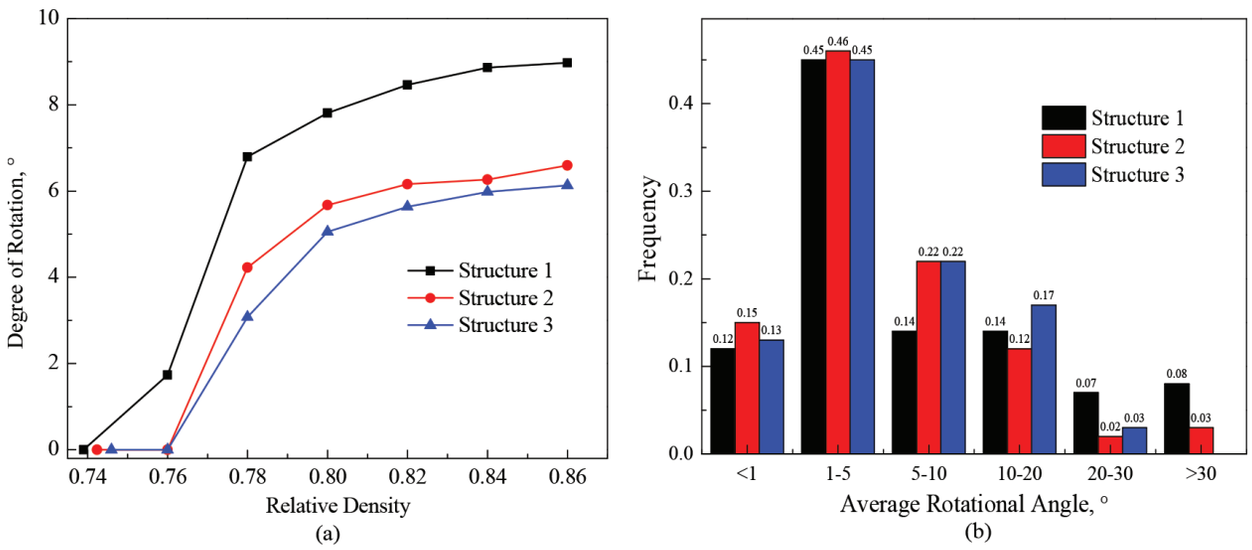

Figure 8. (a) Evolution of average rotational angle with the relative density for each initial packing structure during compaction when the SiC content is 25%; (b) distribution of average rotational angle in the final compacts formed by different initial packing structures.

http://dx.doi.org/10.5772/intechopen.76563

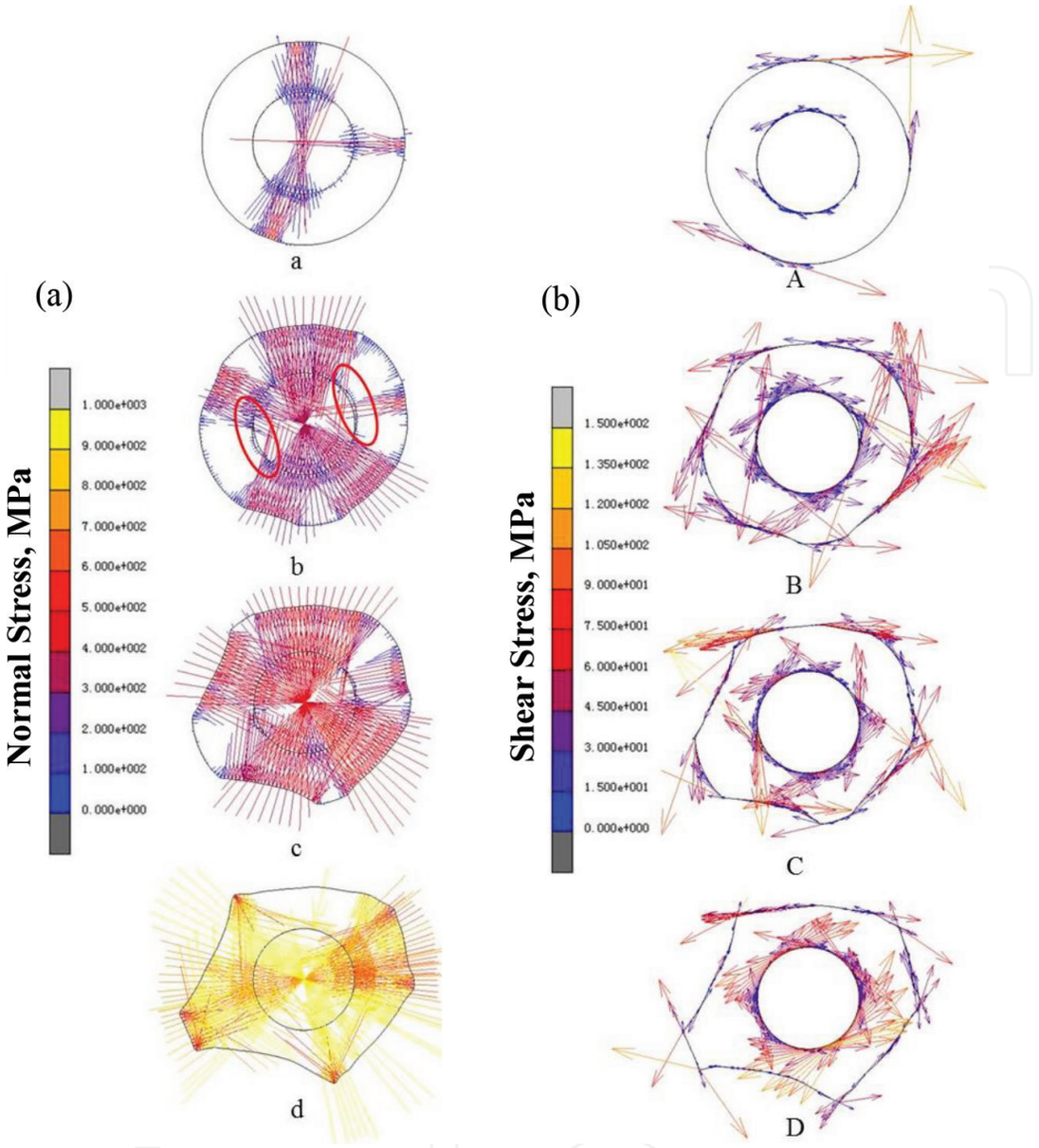

Figure 9. Evolution of (a): normal stress (a–d) and (b): shear stress (A–D) at the interface between Al and SiC of a given core/shell particle when SiC content is 25%. And (a–d)/(A–D) respectively correspond to 800, 1500, 1900, and 2160 incremental modeling steps.

debond unless the SiC content is very large. In order to explain the mechanisms of debonding and rebonding phenomena, a single Al/SiC composite particle in initial random packing is selected for analysis. The evolution of normal stresses and shear stresses in this particle at different stages of compaction is shown in **Figure 9**. As can be imagined from the figure that at the early stage of compaction, composite particles are fully rearranged with the help of relatively low pressure from the upper punch. In this case, no matter the tangential forces or the normal forces between particles or between Al and SiC at the interface are all very small. With the increase of the compaction pressure, the contact forces between composite particles increase. The large extrusion deformation or the shear due to relative sliding induces large tangential stresses at the interface between Al shell and SiC core, when the normal

contact forces or stresses are very small at this region, the debonding occurs. While with the further increase of the compaction pressure, the bulk density of the compact increases. The normal contact forces or stresses at the debonding region increase due to the extrusion from neighboring particles, leading to the rebonding at the interface. Through comparison, one can conclude that the occurrence of debonding phenomenon, which has also been identified in others' work [49], is mainly caused by sufficient tangential forces but insufficient normal forces at the interface. Therefore, the interface should have a certain shear strength and relatively large normal strength, which can not only effectively avoid the possible debonding, but also make the distribution of equivalent strain in the matrix more uniform.

4. Conclusions

DEM-FEM coupled MPFEM modeling on the single action die compaction of Al/SiC core/shell (core: SiC; shell: Al) composite powders with different initial packing structures was conducted from particulate scale in 2D. The effects of compaction pressure, initial packing structure, and SiC content (composition) on the packing densification were systematically presented. Various macro and micro properties such as relative density and distribution, stress and distribution, particle rearrangement through translational motion and rotational motion, deformation and mass transfer, and interfacial behavior between composite particles were characterized and analyzed. Following conclusions can be drawn:

1. MPFEM simulation can effectively reproduce the compaction densification of Al/SiC composite particles with core (SiC)/shell (Al) structures from particulate scale.
2. Beyond a certain Al content, the compaction on both ordered and random initial packings of the composite particles all can realize the full densification, however, the micro properties in these compacts are initial structure sensitive. And the densification rate is also different.
3. The compaction on Al/SiC core/shell composite powders can obtain more uniform relative density and stress distributions than other Al/SiC composite systems.
4. During compaction on random initial packings of Al/SiC composite powders, obvious particle rotations can be observed with the relative density of the compact between 0.74–0.82, and the value of average rotational angles is also affected by the initial packing structure.
5. The debonding between SiC core and Al shell during compaction on random initial packings mainly occurs at the area close to the large pore, where the normal stress is small and the shear stress is relatively large. To avoid it, sufficient normal stress at the core/shell contact area should be satisfied. For the compaction on ordered initial packing such as SC and HCP structures, debonding mainly appears close to the punches when the SiC content is relatively high, and it will be disappeared in the final stage of compaction.

The researches can not only enhance people's understanding on the compaction densification of Al/SiC composite powders with core/shell structures and various initial packing states, but

also provide the materials scientists and engineers with valuable references for the realization of high performance Al/SiC compact in future PM production.

Acknowledgements

The authors are grateful to National Natural Science Foundation of China (No. 51374070) and Fundamental Research Funds for the Central Universities of China (No. N162505001) for the financial support of current work.

Conflict of interest

We declare that we have no conflicts of interest to this work.

Nomenclature

Scalars

A	strength coefficient
B	material constant
E	Young's modulus
m	work hardening index
N	incremental modeling step
n	material constant
O	center of a circle
P	compaction pressure
r	radius of SiC particle
R	radius of Al/SiC composite particle
R^2	relative coefficient
U	constant
v	velocity
x	coordinate on X axis
y	coordinate on Y axis
Z	constant

Greek letters

α	angle
β	angle
Δ	triangle
ε	strain
ε_{ij}	strain tensor
$\dot{\bar{\varepsilon}}$	equivalent strain rate
$\bar{\varepsilon}$	equivalent strain
θ	angle
μ	frictional coefficient
ν	Poisson's ratio
ρ	relative density
ρ_c	relative density of the compact
σ	stress

Subscripts

0	initial time
1	spatial direction
2	spatial direction
3	spatial direction
A	spatial point
A′	spatial point
B	spatial point
B′	spatial point
c	compact
i	integer, ranging from 1 to 3
j	integer, ranging from 1 to 3
p	particulate
y	yield

Acronyms

2D	two-dimensional
CIPed	cold isostatic pressed
DEM	discrete element method
ECAPT	equal channel angular pressing and torsion
FEM	finite element method
HIPed	hot isostatic pressed
MPFEM	multi-particle finite element method
PM	powder metallurgy
PRMMCs	particulate reinforced metal matrix composites
vol.	volume
wt.	weight

Author details

Xizhong An*, Yu Liu, Fen Huang and Qian Jia

*Address all correspondence to: anxz@mail.neu.edu.cn

School of Metallurgy, Northeastern University, Shenyang, PR China

References

[1] Ling CP, Bush MB, Perera DS. The effect of fabrication techniques on the properties of Al-SiC composites. Journal of Materials Processing Technology. 1995;**48**:325-331. DOI: 10.1016/0924-0136(94)01665-N

[2] Tavakoli AH, Simchi A, Seyed Reihani SM. Study of the compaction behavior of composite powders under monotonic and cyclic loading. Composites Science and Technology. 2005;**65**:2094-2104. DOI: 10.1016/j.compscitech.2005.05.016

[3] Prasad Reddy A, Vamsi Krishna P, Narasimha Rao R, Murthy NV. Silicon carbide reinforced aluminium metal matrix nano composites – A review. Materials Today: Proceedings. 2017;**4**:3959-3971

[4] Lloyd DJ, Lagace H, McLeod A, Morris PL. Microstructural aspects of aluminium-silicon carbide particulate composites produced by a casting method. Materials Science and Engineering: A. 1989;**107**:73-80. DOI: 10.1016/0921-5093(89)90376-6

[5] Sridhar I, Fleck NA. Yield behavior of cold compacted composite powders. Acta Materialia. 2000;**48**:3341-3352. DOI: 10.1016/S1359-6454(00)00151-8

[6] Tang F, Hagiwara M, Schoenung JM. Formation of coarse-grained inter-particle regions during hot isostatic pressing of nanocrystalline powder. Scripta Materialia. 2005;**53**:619-624. DOI: 10.1016/j.scriptamat.2005.05.034

[7] Tang F, Hagiwara M, Schoenung JM. Microstructure and tensile properties of bulk nanostructured Al-5083/SiC_p composites prepared by cryomilling. Materials Science and Engineering: A. 2005;**407**:306-314. DOI: 10.1016/j.msea.2005.07.056

[8] Jamaati R, Amirkhanlou S, Toroghinejad MR, Niroumand B. Effect of particle size on microstructure and mechanical properties of composites produced by ARB process. Materials Science and Engineering: A Structural. 2011;**528**:2143-2148. DOI: 10.1016/j.msea.2010.11.056

[9] Ghiţă C, Popescu IN. Experimental research and compaction behavior modelling of aluminium based composites reinforced with silicon carbide particles. Computational Materials Science. 2012;**64**:136-140. DOI: 10.1016/j.commatsci.2012.05.031

[10] Li P, Zhang X, Xue KM, Li X. Effect of equal channel angular pressing and torsion on SiC-particle distribution of SiC_p-Al composites. Transactions of the Nonferrous Metals Society of China. 2012;**22**:s402-s407. DOI: 10.1016/S1003-6326(12)61738-5

[11] Moazami-Goudarzi M, Akhlaghi F. Effect of nanosized SiC particles addition to CP Al and Al-Mg powders on their compaction behavior. Powder Technology. 2013;**245**:126-133. DOI: 10.1016/j.powtec.2013.04.025

[12] Zakaria HM. Mocrostructural and corrosion behavior of Al/SiC metal matrix composites. Ain Shams Engineering Journal. 2014;**5**:831-838. DOI: 10.1016/j.asej.2014.03.003

[13] El-Kady O, Fathy A. Effect of SiC particle size on the physical and mechanical properties of extruded Al matrix nanocomposites. Materials & Design. 2014;**54**:348-353. DOI: 10.1016/j.matdes.2013.08.049

[14] Majzoobi GH, Atrian A, Enayati MH. Tribological properties of Al7075-SiC nanocomposite prepared by hot dynamic compaction. Composite Interfaces. 2015;**22**:579-593. DOI: 10.1080/09276440.2015.1055955

[15] Zhang L, Xu HQ, Wang Z, Li QG, Wu JY. Mechanical properties and corrosion behavior of Al/SiC composites. Journal of Alloys and Compounds. 2016;**678**:23-30. DOI: 10.1016/j.jallcom.2016.03.180

[16] Bajpai G, Purohit R, Rana RS, Rajpurohit SS, Rana A. Investigation and testing of mechanical properties of Al-nano SiC composites through cold isostatic compaction process. Materials Today: Proceedings. 2017;**4**:2723-2732

[17] Penchal Reddy M, Shakoor RA, Parande G, Manakari V, Ubaid F, Mohamed AMA, Gupta M. Enhanced performance of nano-sized SiC reinforced Al metal matrix nanocomposites synthesized through microwave sintering and hot extrusion techniques. Progress in Natural Science. 2017;**27**:606-614. DOI: 10.1016/j.pnsc.2017.08.015

[18] Biswas K. Comparison of various plasticity models for metal powder compaction processes. Journal of Materials Processing Technology. 2005;**166**:107-115. DOI: 10.1016/j.jmatprotec.2004.08.006

[19] Khoei AR, Azami AR, Azizi S. Computational modeling of 3D powder compaction processes. Journal of Materials Processing Technology. 2007;**185**:166-172. DOI: 10.1016/j.jmatprotec.2006.03.122

[20] Eksi AK, Yuzbasioglu AH. Effect of sintering and pressing parameters on the densification of cold isostatically pressed Al and Fe powders. Materials & Design. 2007;**28**:1364-1368. DOI: 10.1016/j.matdes.2006.01.018

[21] Tahir SM, Ariffin AK, Anuar MS. Finite element modelling of crack propagation in metal powder compaction using Mohr-coulomb and elliptical cap yield criteria. Advanced Powder Technology. 2010;**202**:162-170. DOI: 10.1016/j.powtec.2010.04.033

[22] Diarra H, Mazel V, Busignies V. FEM simulation of the die compaction of pharmaceutical products: Influence of visco-elastic phenomena and comparison with experiments. International Journal of Pharmaceutics. 2013;**453**:389-394. DOI: 10.1016/j.ijpharm.2013.05.038

[23] An XZ, Xing ZT, Jia CC. Cold compaction of copper powders under mechanical vibration and uniaxial compression. Metallurgical and Materials Transactions A: Physical Metallurgy and Materials Science. 2014;**45**:2171-2179. DOI: 10.1007/s11661-013-2160-6

[24] An XZ, Zhang YL, Zhang YX, Yang S. Finite element modeling on the compaction of copper powder under different conditions. Metallurgical and Materials Transactions A: Physical Metallurgy and Materials Science. 2015;**46A**:3744-3752. DOI: 10.1007/s11661-015-2929-x

[25] Han P, An XZ, Zhang YX, Zou ZS. FEM modeling on the compaction of Fe and Al composite powders. Journal of Mining and Metallurgy, Section B: Metallurgy. 2015;**51**:163-171. DOI: 10.2298/JMMB150210020H

[26] An XZ, Yang RY, Dong KJ, Zou RP, Yu AB. Micromechanical simulation and analysis of one-dimensional vibratory sphere packing. Physical Review Letters. 2005;**95**:205502-1-205502-4. DOI: 10.1103/PhysRevLett.95.205502

[27] Yu AB, An XZ, Zou RP, Yang RY, Kendall K. Self-assembly of particles for densest packing by mechanical vibration. Physical Review Letters. 2006;**97**:265501-1-265501-4. DOI: 10.1103/PhysRevLett.97.265501

[28] Wu YL, An XZ, Yu AB. DEM simulation of cubical particle packing under mechanical vibration. Powder Technology. 2017;**314**:89-101. DOI: 10.1016/j.powtec.2016.09.029

[29] Zhao B, An XZ, Wang Y, Qian Q, Yang XH, Sun XD. DEM dynamic simulation of tetrahedral particle packing under 3D mechanical vibration. Powder Technology. 2017;**317**:171-180. DOI: 10.1016/j.powtec.2017.04.048

[30] Martin CL, Bouvard D. Isostatic compaction of bimodal powder mixtures and composites. International Journal of Mechanical Sciences. 2004;**46**:907-927. DOI: 10.1016/j.ijmecsci.2004.05.012

[31] Procopio AT, Zavaliangos A. Simulation of multi-axial compaction of granular media from loose to high relative densities. Journal of the Mechanics and Physics of Solids. 2005;**53**:1523-1551. DOI: 10.1016/j.jmps.2005.02.007

[32] Frenning G. An efficient finite/discrete element procedure for simulating compression of 3D particle assemblies. Computer Methods in Applied Mechanics and Engineering. 2008;**197**:4266-4272. DOI: 10.1016/j.cma.2008.05.002

[33] Lee KH, Lee JM, Kim BM. Densification simulation of compacted Al powders using multi-particle finite element method. Transactions of the Nonferrous Metals Society of China. 2009;**19**:s68-s75

[34] Zhang J. A study of compaction of composite particles by multi-particle finite element method. Composites Science and Technology. 2009;**69**:2048-2053. DOI: 10.1016/j.compscitech.208.11.020

[35] Frenning G. Compression mechanics of granule beds: A combined finite/discrete element study. Chemical Engineering Science. 2010;**65**:2464-2471. DOI: 10.1016/j.ces.2009.12.029

[36] Jerier JF, Hathong B, Richefeu V, Chareyre B, Imbault D, Donze FV, Doremus P. Study of cold powder compaction by using discrete element method. Powder Technology. 2011;**208**:537-541. DOI: 10.1016/j.powtec.2010.08.056

[37] Harthong B, Imbault D, Dorémus P. The study of relations between loading history and yield surfaces in powder materials using discrete finite element simulations. Journal of the Mechanics and Physics of Solids. 2012;**60**:784-801. DOI: 10.1016/j.jmps.2011.11.009

[38] Harthong B, Jérier JF, Richefeu V, Chareyre B, Dorémus P, Imbault D, Donzé FV. Contact impingement in packings of elastic-plastic spheres, application to powder compaction. International Journal of Mechanical Sciences. 2012;**61**:32-43. DOI: 10.1016/j.ijmecsci.2012.04.013

[39] Gustafsson G, Häggblad HÅ, Jonsén P. Multi-particle finite element modelling of the compression of iron ore pellets with statistically distributed geometric and material data. Powder Technology. 2013;**239**:231-238. DOI: 10.1016/j.powtec.2013.02.005

[40] Güner F, Cora ÖN, Sofuoğlu H. Numerical modeling of cold powder compaction using multi particle and continuum media approaches. Powder Technology. 2015;**271**:238-247. DOI: 10.1016/j.powtec.2014.11.008

[41] Zhang YX, An XZ, Zhang YL. Multi-particle FEM modeling on microscopic behavior of 2D particle compaction. Applied Physics A: Materials Science & Processing. 2015; **118**:1015-1021. DOI: 10.1007/s00339-014-8861-x

[42] Han P, An XZ, Zhang YX, Huang F, Yang TX, Fu HT, Yang XH, Zou ZS. Particulate scale MPFEM modeling on compaction of Fe and Al composite powders. Powder Technology. 2017;**314**:69-77. DOI: 10.1016/j.powtec.2016.11.021

[43] Han P, An XZ, Wang DF, Fu HT, Yang XH, Zhang H, Zou ZS. MPFEM simulation of compaction densification behavior of Fe-Al composite powders with different size ratios. Journal of Alloys and Compounds. 2018;**741**:473-481. DOI: 10.1016/j.jallcom.2018.01.198

[44] Huang F, An XZ, Zhang YX, Yu AB. Multi-particle FEM simulation of 2D compaction on binary Al/SiC composite powders. Powder Technology. 2017;**314**:29-48. DOI: 10.1016/j.powtec.2017.03.017

[45] An XZ, Yang RY, Zou RP, Yu AB. Effect of vibration condition and inter-particle frictions on the packing of uniform spheres. Powder Technology. 2008;**188**:102-109. DOI: 10.1016/j.powtec.2008.04.001

[46] Heckel RW. Density-pressure relationships in powder compaction. Transactions of the Metallurgical Society of the American Institute of Mechanical Engineers. 1961;**221**:671-675. DOI: 10.1016/0026-0657(92)90966-1

[47] Ramberger R, Burger A. On the application of the Heckel and Kawakita equations to powder compaction. Powder Technology. 1985;**43**:1-9. DOI: 10.1016/0032-5910(85)80073-5

[48] German RM. Particle Packing Characteristics. 2nd ed. Princeton: Metal Powder Industries Federation; 1989. pp. 34-38. DOI: 10.1016/0032-5910(90)80071-6

[49] Haddadi H, Teodosiu C. 3D-analysis of the effect of interfacial debonding on the plastic behavior of two-phase composites. Computational Materials Science. 1999;**16**:315-322. DOI: 10.1016/S0927-0256(99)00074-9

IntechOpen